

Explaining the Variations in Isotopic Ratios in Meteoritic Amino Acids

Michael A. Famiano^{*1,2,3}, Richard N. Boyd^{†4}, Toshitaka Kajino^{‡2,3,5},
Satoshi Chiba^{§3,6}, Yirong Mo^{¶7}, Takashi Onaka^{||8,9}, and Toshio
Suzuki^{** 2,10}

¹Dept. of Physics and Joint Institute for Nuclear Astrophysics, Western Michigan University, 1903 W. Michigan Avenue, Kalamazoo, MI 49008-5252, USA

²National Astronomical Observatory of Japan, 2-21-1 Mitaka, Tokyo 181-8588 Japan

³School of Physics, Beihang Univ. (Beijing Univ. of Aeronautics and Astronautics), Beijing 100083, P.R. China

⁴Department of Physics, Department of Astronomy, The Ohio State University, Columbus, OH 43210 USA

⁵Graduate School of Science, Univ. of Tokyo, 7-3-1 Hongo, Bunkyo-ku, Tokyo 113-0033 Japan

⁶Laboratory for Advanced Nuclear Energy, Institute of Innovative Research, Tokyo Institute of Technology, 2-12-1-N1-16 Ookayama, Meguro-ku, Tokyo, 152-8550, Japan

⁷Department of Chemistry, Western Michigan University, Kalamazoo, MI 49008-5252 USA

⁸Dept. of Astronomy, Graduate School of Science; Univ. of Tokyo, 7-3-1 Hongo, Bunkyo-ku, Tokyo 113-0033 Japan

⁹Dept. of Physics, Meisei University, 2-2-1 Hodokubo, Hino, Tokyo 191-8506, Japan

¹⁰Department of Physics, Nihon University, 3-25-40, Setagaya-ku, Tokyo 156-8550, Japan

May 13, 2020

*Corresponding Author: michael.famiano@wmich.edu, 269-387-4931

†richard11boyde@comcast.net

‡kajino@nao.ac.jp

§chiba.satoshi@nr.titech.ac.jp

¶yirong.mo@wmich.edu

||onaka@astron.s.u-tokyo.ac.jp

**suzuki@phys.chs.nihon-u.ac.jp

Abstract

Measurements of the isotopic abundances in meteoritic amino acids have found enhancements of $^2\text{H}/\text{H}$, $^{15}\text{N}/^{14}\text{N}$, and $^{13}\text{C}/^{12}\text{C}$ in the amino acids in the meteorites studied. We show that they are consistent with the processing of the constituents of the meteorites by electron anti-neutrinos that would be expected from a core-collapse supernova or neutron-star merger. Using theoretical electron anti-neutrino cross sections we are able to predict these isotopic ratio variations depending on the time-integrated anti-neutrino flux at the site where the amino acids were processed.

Keywords: interstellar molecules, meteors, chirality, homochirality

1 Introduction

One of Nature's curiosities is the isotopic abundances observed in the constituents of the amino acids found in meteorites. Specifically, ^{13}C is enhanced slightly over its cosmic abundance, ^{15}N considerably more, and ^2H is greatly enhanced. An additional feature is the fact that these amino acids tend to be slightly skewed toward left-handedness. Since this is as observed nearly in totality in Earthly amino acids (except for the achiral glycine) this has been used to suggest that meteorites may have provided the seeds for the ultimate production of Earthly amino acids.

In earlier work we studied a model by which the left-handedness might have been produced. In this paper we extend that model to study how isotopic ratios variations may be created in meteorites.

Several explanations have been given as to the origin of cosmic handedness selection (e.g. Kojo, 2010; Breslow, 2011; Sojo, 2015; Gleiser and Walker, 2012; Kobayashi, 2019; Rivera Islas et al., 2004; Podlech, 2001; Boyd and Famiano, 2018; Meierhenrich, 2008). In this paper we observe that one model, the Supernova Neutrino Amino Acid Processing (SNAAP) Model, can explain both the handedness

selection and the differences in isotopic abundances in a self-consistent way. Since the SNAAP Model's handedness selection capability has been the subject of many papers (Boyd et al., 2018a; Famiano et al., 2018b; Boyd et al., 2018b; Famiano et al., 2018a, 2017; Famiano and Boyd, 2017), this work will focus on its ability to explain the differences in isotopic abundances.

In the next section we give a brief description of the SNAAP model, including a short discussion of some of its results for amino acid handedness. Section 3 describes our calculations of the isotopic ratios, first describing that for ^2H , then using those results to determine the level of variation for ^{13}C and ^{15}N . We also mention the possibility of Li and B abundance ratios in the same meteorites.

At the end of the results section, we evaluate some of the uncertainties in our computations. Results of our computations are compared to data for meteoroids assuming isotopic abundance distributions corresponding to both the current solar system isotopic abundance distributions and the solar system isotopic abundance distribution 4.6 billion years ago (Gya), where isotopic abundances were taken from Lodders et al. (2009). We show that an evaluation of meteoroids with abundance distributions matching those of the solar system 4.6 Gya gives the most reasonable agreement with observed values of ratios in D/H, $^{15}\text{N}/^{14}\text{N}$, and $^{13}\text{C}/^{12}\text{C}$ ratios. The reason for this may be because meteoric isotopic abundances *prior to* irradiation likely more closely matched those of the early solar system.

Finally we give our conclusions. Here, we provide future perspectives and plans as well as well as an iteration of the importance of sample return missions. In addition, we note the importance and past work in low-temperature chemistry (particularly D enhancement) (Elsila et al., 2012) in interpreting measured values. The

model presented here may complement existing interpretations.

2 The SNAAP Model

In this model (Boyd et al., 2018a; Famiano et al., 2018b; Boyd et al., 2018b; Famiano et al., 2018a, 2017; Boyd and Famiano, 2018; Famiano and Boyd, 2017), meteoroids might be processed in the intense magnetic field and electron anti-neutrino (hereafter denoted anti-neutrino) flux from one of several stellar objects. The anti-neutrinos are selective in their destruction of the amino acids as they are purely chiral (assuming massless anti-neutrinos), a result of the weak interaction nuclear physics that describes their interaction with the ^{14}N nuclei. The relevant nuclear reaction is



where $\bar{\nu}_e$ is an electron anti-neutrino and e^+ is an anti-electron, a positron. If the $\bar{\nu}_e$ spin (1/2, in units of \hbar , Plancks constant divided by 2π) is antiparallel to that of the ^{14}N (spin 1), then a total spin on the left-hand side of the equation is either 1/2 or 3/2. The smaller value will equal the sum of the spins of ^{14}C (spin 0) and the positron (spin 1/2) on the right-hand side, thus conserving angular momentum. However, if the $\bar{\nu}_e$ spin and the ^{14}N spin are aligned, conservation of angular momentum will require one additional unit of angular momentum to come from either the $\bar{\nu}_e$ or the e^+ wave function in order for the total angular momentum on the right-hand side to equal the 3/2 on the left-hand side. This is known from basic nuclear physics (Famiano et al., 2018b) to introduce roughly an order of magnitude smaller cross section for the latter case compared to the former. However, this also introduces

a parity change. Since the transition from ^{14}N to the ^{14}C ground state is between nuclear states of the same parity, two units of angular momentum must therefore come from the anti-neutrino and/or positron wave functions. Thus the inhibition may be closer to two orders of magnitude. This spin-dependent reaction probability is the origin of the effect predicted for the SNAAP model.

Detailed quantum molecular calculations (Famiano et al., 2018a,b) have shown that the complex interactions of the molecules with the intense magnetic field of a neutron star or a two neutron star merger and the effective electric field caused by the motion of the meteoroids through the magnetic field, a result of the Lorentz force, do produce an environment that is truly chiral (Barron, 2008). In this situation, the interaction of the ^{14}N nuclei with the $\bar{\nu}_e$ s is chirally selective, and will in many cases, destroy more of the right-handed amino acids than the left-handed ones (Famiano et al., 2018a).

The external magnetic field aligns the ^{14}N nuclei via their nuclear magnetic moments, whereas the effective electric field aligns the molecular electric dipole moments, which depend on the chirality. The external magnetic field, however, is modified at the nucleus by the effects of the orbital electrons, known as shielding. This, in turn causes a chirality sensitive perturbation on the magnetic orientation of the nuclei, which leads to a chirality-dependent magnetization (a bulk property).

These components exist even without the coupling to the electric dipole moment (Buckingham and Fischer, 2006; Famiano et al., 2018a), but that coupling enhances the difference between the angles that the two chiral states make with the anti-neutrino spin, hence of the chirality selective destruction of the amino acids (Famiano et al., 2018b,a). From the magnitude of these effects, one can determine

the enantiomeric excesses, ees , ($ee = (N_L - N_D)/(N_L + N_D)$, where N_L (N_D) is the number of left-handed (right-handed) amino acids in any ensemble) that might be expected for amino acids from the SNAAP model. Ees on the order of percents are predicted for a variety of parameters in this model.

At least two sites seem promising for producing the effects we have studied: a supernova from a star that is in a massive star-neutron star binary and a neutron star-neutron star (NS) merger. Both could produce the anti-neutrino flux and magnetic field needed to process nearby objects such as large meteoroids or planets (the anti-neutrinos would process the entire object regardless of the size). Finally large objects passing by or in highly elliptical orbits would be necessary to limit the exposure to the high temperature near the central object. These have been discussed in previous work (Boyd et al., 2018; Boyd and Famiano, 2018).

Since life began on Earth more than 4 billion years ago, the detritus from such an event would have to have gotten to earth prior to that time. A supernova could have both created the processed amino acids and a shock wave that precipitated the solar system. A supernova subsequent to formation of the Solar System could also have sent amino acid laden debris to Earth. Such an event apparently deposited ^{60}Fe (half-life of 1.5 Myr) on Earth roughly one million years ago (Koll et al., 2019), suggesting such depositions might well have provided the appropriately processed meteorites.

In principle, electron neutrinos could drive the ^{14}N to ^{14}O , but the threshold energy is much higher for this reaction (greater than 5 MeV compared to much less than 1 MeV). Since the cross section for neutrino capture processes increases sharply with the energy above threshold, and the anti-neutrino energies expected

(Rosswog and Liebendörfer, 2003) from coalescing neutron stars are predicted to be much larger for anti-neutrinos than neutrinos (16 MeV versus 10 MeV), this reaction does not have a large effect on the enantiomerism that results from the combined flux from anti-neutrinos and neutrinos in that site.

3 Materials and Methods

3.1 Estimating Isotopic Ratios in Amino Acids

The variations in isotopic abundances in the nuclei of the amino acids were estimated by assuming initial mass fractions equal to those found in solar system meteoric mass fractions taken from Lodders (2009). Initial mass fractions were used for the solar system average, the Orgueil meteorite, and the solar system at formation (4.6 Gya). Exposure to an anti-neutrino flux from a nearby source was then assumed. The neutrino energies and temperatures used for three models are indicated in Table 1. These values were taken from the Rosswog and Liebendörfer (Rosswog and Liebendörfer, 2003) evaluation of NS mergers and are representative of typical neutrino luminosity and temperatures in such an event.

Neutrino and anti-neutrino charged-current (CC) and neutral-current (NC) interactions, as well as electron captures and β decays, have been included in a simple network to compute the changes in isotopic abundance as a function of time for a neutrino flux from a given source.

The isotopic abundance enhancements or deficiencies are evaluated by comparing to standards (VPDB for ^{13}C (Hut, 1987), VSMOW for D (Hagemann et al., 1970; de Wit et al., 1980), and air for ^{15}N (Junk and Svec, 1958)) used in meteoric

analysis. The standard δ notation used to evaluate isotopic abundance is:

$$\delta^A \equiv \left[\frac{R(A)_{sample}}{R(A)_{standard}} - 1 \right] \times 1000\text{‰} \quad (2)$$

where $R(A)$ is the abundance ratio of an isotope of mass A to the most abundant isotope of the same element.

For the present calculations, the reaction network was run for up to 10 s. The values of δ were computed at each time step in the evaluation.

3.2 Model Parameters

3.2.1 Meteoroid Parameters

The initial elemental abundances in the model meteoroid correspond to the CI abundances of the Orgueil meteorite rock average as stated in Lodders et al. (2009) with isotopic distributions for individual elements taken to be that of the solar system 4.6 billion years ago (Table 10 from the same reference). Additionally, two other abundance distributions were chosen to match the abundance distribution of the solar system at formation (Lodders et al., 2009) and the currently suggested solar photospheric values (Lodders et al., 2009).

Although amino acids within meteoric inclusions are not necessarily homogeneously distributed, it is safe to assume a homogeneously mixed meteoroid for the following reasons. Here, we use the term *inclusion* to indicate any inhomogeneity within the parent body, including cavities and pockets of water. This is a more general definition than in some literature (Chizmadia et al., 2002; Brearley, 1999; Pizzarello and Shock, 2010). In the current work, we are assuming that any inclu-

sion is $\lesssim 1$ mm in size, similar in size to grains and chondrules studied in carbonaceous chondrites (Chizmadia et al., 2002; Brearley, 1999; Pizzarello and Shock, 2010). The anti-neutrinos will penetrate and process the entire meteorite evenly. Any neutrons that are produced will have an initial mean free path of a few centimeters, which is much larger than the expected size of the inclusions. For this reason, neutrons produced in the vicinity of the inclusions will penetrate the volume of the meteoroid. Neutrons produced within and without the inclusions were thus assumed to be uniformly distributed in energy and space.

3.2.2 Nuclear Reaction Network

Two reaction networks were used in this analysis. Neutrino CC and NC reactions were evaluated using the network of Figure 1 (Meyer, 2012). Each black line in the figure is a possible neutrino capture reaction path. For example, the reaction $^{12}\text{C} + \nu_{\mu} \rightarrow ^{11}\text{C} + \text{n} + \nu'_{\mu}$ would be represented by a black line. The dominant β^{\pm} decays are represented by red lines. Stable nuclei are shaded in yellow. After the neutrino burst, post-processing by neutrons produced via anti-neutrino captures on hydrogen and NC reactions was incorporated into a network of species with $Z \leq 26$. We base this choice on the assumption that the environment was cold enough and sparse enough that only neutrino and neutron capture reactions occurred, and they did so at low enough rates that the neutron captures were decoupled from the neutrino captures. Under these conditions, it is unlikely that any particular species will undergo multiple sequential captures.

The anti-neutrino luminosities and temperatures specified in Table 1 were presumed constant throughout the duration of the burst. Neutrino NC and CC cross

sections were taken from the literature (Kolbe et al., 2003; Meyer et al., 1998; Strumia and Vissani, 2003; Suzuki et al., 2018; Woosley et al., 1990) where available. For the low-mass Li and B isotopes, cross-sections were evaluated using the shell-model calculations of Suzuki et al. (2006).

3.2.3 Neutron Captures and Post-Processing

Subsequent neutron captures are energy-dependent. Neutron captures on all isotopes present in the meteoroid up to ^{56}Fe were evaluated and were taken from the ENDF compilation (ENDF/B-VIII) (Brown et al., 2018). Here, the fraction of neutrons F_i captured on a species i during thermalization is:

$$F_i = \frac{n_i \int_{E_o}^{\langle E \rangle} \sigma_i(E) \phi_{IBD}(E) dE}{\sum_i n_i \int_{E_o}^{\langle E \rangle} \sigma_i(E) \phi_{IBD}(E) dE} \quad (3)$$

where $\langle E \rangle$ is the average energy of the produced neutrons, and n_i is the number density of species i . The integration is over the entire energy spectrum of the neutrons as they thermalize to a presumed lower energy E_o , which is taken to be 25 meV, low enough such that the cross-sections of all neutrons at this energy are dominated by non-resonant capture. The neutron energy spectrum, $\phi_{IBD}(E)$, is taken to be that of proton inverse β decay (IBD), which is determined based on the energy distribution of neutrons produced in IBD and thermalized in the intervening meteoric rock.

This assumes that the neutron scattering cross sections are dominant in the thermalization process. Otherwise, a correction to the integrals would require a shift in the neutron energy-dependent flux as neutrons are also captured as they thermalize. However, since most of the captures occur at lower energies during the thermaliza-

tion process, where the relative rates scale only by the thermal neutron capture cross sections, the effect of the treatment given by Equation 3 is to correct for resonances at higher energy, where the capture cross section is much less than the scattering cross section.

The energy loss rate $\frac{dE}{dx}$ is taken from the inelastic scattering cross section of neutrons in material. From this, the energy loss rate can be calculated assuming a constant scattering cross section of ≈ 5 b and an average energy loss per collision of $f=0.9$ of the original energy (Krane, 1987). The energy loss rate is then given by:

$$\begin{aligned}
 E &= E_0 f^{x/\lambda} & (4) \\
 &= E_0 e^{\alpha x} \\
 \rightarrow \frac{dE}{dx} &\propto e^{\alpha x}
 \end{aligned}$$

where λ is the mean free path of neutrons in the material. In this case, λ is estimated to be 5 cm, although it depends on the composition and density of the material. As mentioned in §3.2.1, we can take this as an average over the entire meteoroid. While the energy loss rate may be higher for aqueous inclusions, the inclusions are so small that the neutrons will not thermalize significantly within them. That is, $\lambda_n \gg r_i$, where λ_n is the neutron mean-free-path (in either water or rock) and r_i is the inclusion radius. With this condition satisfied, the meteoroid may be treated as homogeneous.

In order to properly evaluate the neutron average energy used in Equation 3, the energy distribution of neutrons from the NC and proton inverse beta decay must be calculated. For the proton inverse beta decay, nearly all of the excess kinetic energy

is carried by the positron. For the electron anti-neutrino energies listed in Table 1, the neutron energy is roughly 200 keV (Strumia and Vissani, 2003). The produced neutrons will then penetrate the surrounding medium, including the rock and any intervening organic material, losing energy as they proceed.

Nearly 100% of all of the neutrons produced in the reaction network come from inverse beta decay of the proton, given that the charged-current cross section is several orders of magnitude larger than the neutral current nuclear cross sections evaluated and the H abundance in the meteoric medium is significant. Thus, we assumed average neutron energies corresponding to those emitted in charged-current reactions with hydrogen.

4 Results

Isotopic abundances have been determined for all species in the reaction network. Comparisons have been made to the meteoric measurements of Elsila et al. (Elsila et al., 2012). The results are shown in Figures 2 - 4.

In all figures, the red, green, and purple lines show the calculated results based on models C, D, and E of Table 1, where each curve is a parametric line in time (corresponding to increasing neutrino fluence). That is, for each line in the figure, neutrino exposure time increases from the lowest values of the isotopic ratios to the highest values. The direction of increasing exposure time (fluence) is indicated in Figure 2. Because a constant neutrino flux is assumed, increasing time corresponds

to increasing integrated flux (fluence):

$$\mathcal{F}(t) \equiv \int \phi(t) dt \quad (5)$$

As the exposure time and fluence are variable, any point on the lines in the figures represents a valid possible set of isotopic ratios.

This is important to note for the following reason. While the computation assumes constant flux, for the strong neutrino flux assumed, the neutrino interactions dominate over other reactions in the short timescale noted here. In evaluating the values of δ , we have assumed that all unstable nuclei have decayed back to stability. This means that the points at which the trends indicated by the calculated lines in the figures show the final equilibrium value of δ at a particular fluence.

The measured values in each figure are indicated by the markers. Individual marker types correspond to the meteorite from which the amino acids were extracted. The color of the marker corresponds to the type of meteorite from which the amino acids were extracted. Red, blue, black, and dark yellow markers correspond to CM2, CR2, CR3, and CM1/2 meteorites respectively.

5 Discussion

Several things must be noted in comparing the results of the calculations with the data. First, the data are amino acid specific, which explains the wide range of values they exhibit. However, our calculations involve anti-neutrinos with energies that far exceed molecular binding energies, so they could not possibly be specific to individual amino acids. Thus the results of the calculations must be compared to

some average of the observed values. The arithmetic mean of the data is indicated by the black trefoil mark in Figures 2 - 4.

Second, what our calculations predict is the isotopes produced in reactions that would surely destroy the molecules in which the atoms existed before the interaction occurred. Thus, if the SNAAP model is correct, what the data show is the isotopic ratios in the amino acids that resulted from the recombination of the atoms and amino acid fragments that were produced in the interactions.

Would the newly formed amino acids have a preferred handedness? The environment in which the detritus from the anti-neutrino interactions exists would be ideal for enabling autocatalysis (Glavin et al., 2012; Viedma et al., 2008; Blinova et al., 2014), which might give the newly formed amino acids the same, or even greater, left-handedness than that of the amino acids that were not destroyed by the anti-neutrino interactions. Of course, recombination could occur on vastly larger time scales than the anti-neutrino processing.

Third, we note that the anti-neutrino burst could produce a strong ^{15}N component in the newly formed amino acids. Nitrogen is generally the least abundant atom in the H, C, N, and O atoms that are essential for amino acids. The anti-neutrinos interacting with the more abundant oxygen, especially if water exists in the inclusions, might therefore enhance appreciably the abundance of the amino acids over what existed prior to the anti-neutrino processing. Furthermore, the amino acids would tend to have enhanced D and ^{15}N abundances. Thus the question of the extent to which the newly formed amino acids would achieve some chirality becomes very important.

Finally, the recoiling particles from the anti-neutrino induced reactions would

affect the abundances of atoms that would be available for recombination. The recoiling nuclei would have energies of only a few eV, so would have little effect on the adjacent molecules. The positrons, however, would have MeVs of energy, so could produce many of the constituents of subsequent amino acid formation, especially if water was abundant.

In the absence of information that would lend guidance to the above considerations, the best we could achieve is qualitative agreement between the calculations and the data.

Given these caveats, the computations do compare reasonably to the observed results. The calculations are seen to produce the huge variations in the isotopic ratios for D, ^{15}N , and ^{13}C . The δD of several thousand is obtained in our calculations at the same fluence that gives a $\delta^{15}\text{N}$ of order 150 and a ^{13}C of order 10. Indeed, in Figure 4, with the acknowledgement that the D abundance is likely to be high, the calculations are seen to produce results in fairly good agreement with the indicated data averages at an anti-neutrino fluence within the plausible range. It appears that the D abundance is overestimated in this computation, particularly in Figures 3 and 4. However, produced deuterium would be expected to diffuse out of the inclusions less readily than would ordinary hydrogen (Ganguly, 2002), but both would be expected to diffuse out more readily than N or C. This selective diffusion of H might be partially responsible for the very large δD values in the data. Indeed, this could also explain the fluctuations in the data, as smaller inclusions would be subject to more diffusion than larger ones. These two effects have not been included in our calculations.

It is also important to note that amino acids abundances, isotopic composition,

and enantiomeric excesses may have been affected by aqueous alteration processes (Sephton et al., 2004; Glavin and Dworkin, 2009). This could be responsible for the scatter in the measured isotopic ratios indicated in the figures. Thus, the scatter in measured values - and possibly the values themselves - may be loosely correlated with the type of meteorite from which the amino acids were extracted. For example, measurements of δD appear to cluster near lower values for CR3 and, to a lesser extent, the CR2 meteorites. Further, the CR3 meteorites exhibit a lower range of values of $\delta^{13}C$ than the CM types. These differences in scatter and ranges of values seem to be consistent with the fact that the CR type meteorites are believed to contain the most primitive organic material ((Glavin and Dworkin, 2009)).

The model presented here does not predict or account for any aqueous alteration processes. However, we may be able to draw a loose comparison to the more primitive meteorites studied. In Figure 2, for example, we see that our model E is able to produce lower values of δD , which may compare more favorably to the more primitive meteorites. Likewise, all models are able to predict lower values of $\delta^{13}C$ consistent with the more primitive meteorites.

5.1 Composition of Meteoric Inclusions

Calculations were also performed in which inhomogeneities in the inclusions were assumed. The evaluation of the effects of water on any nuclear processes in the meteorite is rudimentary as the parent body history may vary from one body to the next. The current model would have to reflect the history of a large variety of meteoroids and comets, with potentially large variations in the amount of water contained within them (Alexander et al., 2018; Marty et al., 2016; Jewitt, 2016). Thus

we assume only a single case with inclusions containing water with an assumed water mass fraction of 10%. This might correspond to a body rich in water, but not necessarily the most water-rich body but not necessarily the largest enrichment thought possible (Marty et al., 2016). In this evaluation, the water could be either liquid or ice, since shifts in nuclear species are independent of the chemical phase. Water could take the form of small pockets or “bubbles” in the meteoric inclusions. As stated previously, the nuclear processes studied are independent of the actual molecular species being studied and depend only on the isotopic (nuclear) composition. Any chemical processing would be independent and in addition to the processes studied here.

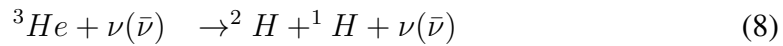
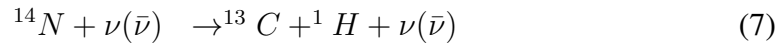
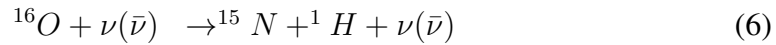
The isotopic fractions assumed for the inclusions are shown in Table 2. The individual isotopic fractions were assumed to be that of the Orgueil meteorite as listed in (Lodders et al., 2009). Initial isotopic ratios (e.g. D/H) were assumed to be those of Table 10 of the same reference. (Note that mass fractions, and not isotopic abundance fractions are indicated in Table 2.) Although this is a high fraction of water, it was used to obtain a qualitative estimate of the effects of aqueous environments on the meteoric abundances.

In order to evaluate isotopic abundances in water inclusions, we assumed that the anti-neutrino flux will initially alter the abundances within the inclusion. However, because of the large mean-free-path of the neutrons, we assumed a subsequent neutron flux of a homogeneously mixed carbonaceous chondrite with a composition consistent with that of the Orgueil meteorite. Thus the neutron abundance and energy for water inclusions is assumed to be the same as that of the meteoroid. Likewise the fraction of neutrons captured in any specific reaction is the same as

average neutron capture rates based on the average composition of meteoric material. Locally (i.e., within the inclusion), the fractional amount of an isotopic species undergoing a reaction is the same as the meteoric average. The absolute amount, however, depends on the local abundance.

The results for this analysis are shown in Figure 5. It can be seen that the results are very similar to those of the Orgueil meteorite, though the values of δD appear somewhat higher. None the less the same qualitative agreement with the Orgueil results as seen without the water inclusion is observed.

Some understanding can be gained from this result by examining the significance of neutron captures, which is shown in Figure 6. Here, the values of δD , $\delta^{13}C$, and $\delta^{15}N$ are shown as a function of time in the neutrino flux if neutron captures are enabled or disabled. In each situation, an isotopic shift is induced either via the neutral current reactions:



or via neutron capture:



In Figure 6, we see that disabling neutron captures results in effectively disabling all deuterium production, while only slightly suppressing ^{13}C and suppressing ^{15}N production somewhat. Thus deuterium is produced almost entirely via the reaction given by Equation 11. The production of ^{15}N proceeds primarily through the reaction given by Equation 9 with a contribution from the reaction given by Equation 6. The production of ^{13}C proceeds primarily via the reaction given by Equation 7.

The inclusion of water increases the initial H and D mass fractions as seen in Table 2, while the remaining mass fractions change by smaller absolute amounts.

It is assumed that the overall average neutron flux does not change even if water inclusions are assumed as most of the neutrons are produced in the surrounding rock. This means that the fraction of H converted to deuterium and the fraction of ^{14}N converted to ^{15}N does not change. However, since the absolute amount of H is larger, the total amount of deuterium produced is also larger.

In the case of ^{15}N , there is some dependence on neutron captures, but also a small dependence on neutral current interactions in producing ^{15}N via the reaction 6. There is little change in the overall ratio, however, because the meteoric material is very rich in oxygen regardless of the inclusion composition and the overall oxygen abundance changes little. Likewise, the N/O ratio in this sample is identical to that of the Orgueil meteorite assumed in Figure 2.

It's also worth noting the timescales in Figure 6. While Figures 2 – 5 show the correlations between isotopic ratios, the time dependence (e.g., which point in the figures corresponds to how much time has elapsed in the model) is not shown explicitly in those figures, while it is present in Figure 6. It is noted that the ratios calculated coincide with the measurements in less than 1 s, which is the approximate

duration of the neutrino flux in a NS merger (Rosswog and Liebendörfer, 2003), one of the postulated sites of this model (Boyd et al., 2018b; Famiano et al., 2018a, 2017; Famiano and Boyd, 2017).

Weak interactions would likely be responsible for a wide variety of differences in isotopic abundance ratios in the same meteorites, specifically D/H , $^{13}C/^{12}C$, $^{15}N/^{14}N$, $^7Li/^6Li$ and $^{10}B/^{11}B$. While Li and B are not present in meteoric amino acids, neutrino interactions in the surrounding rock might be thought to induce similar isotopic abundance changes.

Lithium and boron isotopic ratios have also been studied in meteorites in which amino acid enantiomeric excesses and isotopic enhancements have been found (Seph-ton et al., 2013; Gyngard et al., 2007; Marhas et al., 2002; McDonough et al., 2003). In these studies, variations in the 7Li and ^{10}B isotopic ratios have been observed. Of course, any chemical, thermal, and physical processes for Li and B are independent of any amino acid processing and chemistry. Thus, Li and B processing should be treated independently. However, any meteoroid which contains organic material will also contain other elements, including Li and B. Because of this, any processing of amino acids at the nuclear level also occurs for other elements in the same body.

While we have considered processing of Li and B isotopic ratios, we have found the uncertainties in our calculations to be too great to render an effective, conclusive calculation. We hope to explore processing of Li and B in subsequent studies.

While the evaluation of abundances using the initial meteoritic abundances of the Orgueil meteorite (Lodders et al., 2009) most closely matches current measurements, those initial abundances used were those taken after any presumed pro-

cessing has occurred. It should also be noted that enrichment in L-enantiomers from meteorites are somewhat disputed as terrestrial contamination may have influenced the results. A more accurate evaluation could be done with abundances of a primitive meteorite, or better yet, from samples returned to Earth by Hayabusa2 (Watanabe et al., 2019; Kitazato et al., 2019; Sugita et al., 2019; Jaumann et al., 2019).

6 Conclusions

In previous works (Boyd et al., 2018a; Famiano et al., 2018b; Boyd et al., 2018b; Famiano et al., 2018a, 2017; Famiano and Boyd, 2017; Boyd and Famiano, 2018), the SNAAP model was shown to offer a possible explanation of amino acid chiral selection in stellar environments via parity-violating weak interactions. The quantitative results have suggested that this model could explain the selection of left-handed amino acids in stellar meteorites.

This work shows that this model is not only capable of inducing amino acid chiral selection in meteorites but also produces shifts in isotopic abundance ratios which are comparable to those observed in the same meteorites. Furthermore, the required electron anti-neutrino fluences required in the two situations are comparable.

We studied three scenarios of the presumed neutrino flux and energy spectrum in a neutron-star merger model. Using a nuclear reaction network, we examined the possible change in isotopic abundance ratios in meteoric material. The model used here simultaneously predicts isotopic shifts in both organic material and the

surrounding rock. We emphasize that the predictions in the figures show time evolution of predicted abundance ratios. (That is, each dot in the shown results corresponds to a different integrated flux.) Thus, an observed result should correspond to only one of any of the dots in the figures. While we do not attempt to replicate the scatter in the measurements or any subsequent chemistry, we do note that many of our predictions appear to fall within the locus of observed results.

Of the models studied, Model C of the Rosswog and Liebendörfer (2003) merger model seems to produce abundance distributions most consistent with observations. Of the initial abundance distributions studied, initial abundances matching those of the early solar system result in calculations similar to observed results, though the scatter in measurements is significant.

Though observed values have a large amount of uncertainty, even within a single parent body, we note that our computations here are able to provide results that are within the range of observations. Additionally, because the anti-neutrino fluence varies from one meteoroid to the next, the range of possible values of isotopic ratios between meteoritic measurement can be explained. While we have not explored the chemistry involved, we note that this may also contribute to isotopic variations between models.

The study of weak interactions in selecting amino acid chirality is still quite young, and there are many directions to take. In the case of meteoric abundances, future work will concentrate on careful evaluation of individual astrophysical sites in which this model may work as well as further signatures of this model.

One might also consider the effects on the production of ^{27}Al in similar studies as many of the isotopic ratio measurements pertained to studies of SiC grains. Re-

actions on Si in such grains might also be responsible for ^{27}Al production. Future studies of meteoric samples might want to include this possibility.

It will be especially interesting if Hayabusa2 returns to Earth with sufficiently large samples from asteroid 162173 Ryugu to determine the enantiomeric excesses of the amino acids and the variations in isotopic ratios of the five elements discussed in this paper.

Acknowledgments

MAF is supported by a Moore Foundation grant #7799, the Fulbright Foundation, and by the NAOJ visiting professor program. TK is supported in part by Grants-in-Aid for Scientific Research of JSPS (15H03665, 17K05459). TS is supported in part by JSPS KAKENHI Grant Number JP19K03855. MAF and SC both acknowledge support from a visiting professorship at Beihang University. The authors would also like to thank the anonymous referee for several excellent comments, which have greatly improved this manuscript.

References

- Alexander, C. M. O., McKeegan, K. D., and Altwegg, K. (2018) Water Reservoirs in Small Planetary Bodies: Meteorites, Asteroids, and Comets. *Space Science Rev.* 214:36.
- Barron, L. D. (2008) Chirality and life. *Space Science Reviews* 135:187–201.
- Blinova, A. I., Zega, T. J., Herd, C. D. K., and Stroud, R. M. (2014) Testing variations within the tagish lake meteorite: Mineralogy and petrology of pristine samples. *Meteoritics & Planetary Science* 49:473–502.
- Boyd, R. N. and Famiano, M. A. (2018) *Creating the Molecules of Life*. IOP (London).
- Boyd, R. N., Famiano, M. A., Kajino, T., and Onaka, T. (2018a) A New Paradigm for Creating Amino Acid Chirality. In *American Astronomical Society Meeting Abstracts #232*, volume 232 of *American Astronomical Society Meeting Abstracts*, page 405.05.
- Boyd, R. N., Famiano, M. A., Onaka, T., and Kajino, T. (2018b) Sites that can produce left-handed amino acids in the supernova neutrino amino acid processing model. *Astroph. J.* 856:26.
- Boyd, R. N., Famiano, M. A., Onaka, T., and Kajino, T. (2018) Sites that Can Produce Left-handed Amino Acids in the Supernova Neutrino Amino Acid Processing Model. *apj* 856:26. arXiv: 1802.08285.

Brearley, A. J. (1999) Origin of graphitic carbon and pentlandite in matrix olivines. In *in the Allende meteorite, Science*, pages 1380–1382.

Breslow, R. (2011) The origin of homochirality in amino acids and sugars on pre-biotic earth. *Tetrahedron Letters* 52:4228 – 4232.

Brown, D., Chadwick, M., Capote, R., Kahler, A., Trkov, A., Herman, M., Sonzogni, A., Danon, Y., Carlson, A., Dunn, M., Smith, D., Hale, G., Arbanas, G., Arcilla, R., Bates, C., Beck, B., Becker, B., Brown, F., Casperson, R., Conlin, J., Cullen, D., Descalle, M.-A., Firestone, R., Gaines, T., Guber, K., Hawari, A., Holmes, J., Johnson, T., Kawano, T., Kiedrowski, B., Koning, A., Kopecky, S., Leal, L., Lestone, J., Lubitz, C., Damin, J. M., Mattoon, C., McCutchan, E., Mughabghab, S., Navratil, P., Neudecker, D., Nobre, G., Noguere, G., Paris, M., Pigni, M., Plompen, A., Pritychenko, B., Pronyaev, V., Roubtsov, D., Rochman, D., Romano, P., Schillebeeckx, P., Simakov, S., Sin, M., Sirakov, I., Sleaford, B., Sobes, V., Soukhovitskii, E., Stetcu, I., Talou, P., Thompson, I., van der Marck, S., Welsch-Sherrill, L., Wiarda, D., White, M., Wormald, J., Wright, R., Zerkle, M., Erovnik, G., and Zhu, Y. (2018) Endf/b-viii.0: The 8th major release of the nuclear reaction data library with cielo-project cross sections, new standards and thermal scattering data. *Nuclear Data Sheets* 148:1 – 142. Special Issue on Nuclear Reaction Data.

Buckingham, A. D. and Fischer, P. (2006) Direct chiral discrimination in NMR spectroscopy. *Chemical Physics* 324:111–116.

Chizmadia, L. J., Rubin, A. E., and Wasson, J. T. (2002) Mineralogy and petrology

- of amoeboid olivine inclusions in CO₃ chondrites: Relationship to parent-body aqueous alteration. *Meteoritics & Planetary Science* 37:1781–1796.
- de Wit, J., van der Straaten, C., and Mook, W. (1980) Determination of the absolute hydrogen isotopic ratio of v-smow and slap. *Geostandards Newsletter* 4:33–36.
- Elsila, J. E., Charnley, S. B., Burton, A. S., Glavin, D. P., and Dworkin, J. P. (2012) Compound-specific carbon, nitrogen, and hydrogen isotopic ratios for amino acids in CM and CR chondrites and their use in evaluating potential formation pathways. *Meteoritics and Planetary Science* 47:1517–1536.
- Famiano, M. A. and Boyd, R. N. (2017) *Determining Amino Acid Chirality in the Supernova Neutrino Processing Model*, page 2383. Springer International (Switzerland).
- Famiano, M. A., Boyd, R. N., Kajino, T., and Onaka, T. (2017) Selection of Amino Acid Chirality via Weak Interactions in External Fields. In *XVIIIth International Conference on the Origin of Life*, volume 1967, page 4073.
- Famiano, M. A., Boyd, R. N., Kajino, T., and Onaka, T. (2018a) Selection of Amino Acid Chirality via Neutrino Interactions with ¹⁴N in Crossed Electric and Magnetic Fields. *Astrobiology* 18:190–206.
- Famiano, M. A., Boyd, R. N., Kajino, T., Onaka, T., and Mo, Y. (2018b) Amino Acid Chiral Selection Via Weak Interactions in Stellar Environments: Implications for the Origin of Life. *Scientific Reports* 8:8833.
- Ganguly, J. (2002) Diffusion kinetics in minerals: Principles and applications to tectono-metamorphic processes. In Gramaccioli, C. M., Papp, G., and Weiszburg,

- T., editors, *Energy Modelling in Minerals*, pages 271–309. Mineralogical Society of Great Britain and Ireland, Budapest.
- Glavin, D. P. and Dworkin, J. P. (2009) Enrichment of the amino acid L-isovaline by aqueous alteration on CI and CM meteorite parent bodies. *Proceedings of the National Academy of Science* 106:5487 – 5492.
- Glavin, D. P., Elsila, J. E., Burton, A. S., Callahan, M. P., Dworkin, J. P., Hiltz, R. W., and Herd, C. D. K. (2012) Unusual nonterrestrial l-proteinogenic amino acid excesses in the tagish lake meteorite. *Meteoritics & Planetary Science* 47:1347–1364.
- Gleiser, M. and Walker, S. I. (2012) Life's chirality from prebiotic environments. *International Journal of Astrobiology* 11:287–296.
- Gyngard, F., Amari, S., Zinner, E., Gallino, R., and Lewis, R. S. (2007) Lithium, Boron, and Sulphur Isotopic Ratios in Large Presolar SiC Grains from Murchison. In *Lunar and Planetary Science Conference*, page 1963.
- Hagemann, R., Nief, G., and Roth, E. (1970) Absolute isotopic scale for deuterium analysis of natural waters. absolute d/h ratio for snow. *Tellus* 22:712–715.
- Hut, G. (1987) Consultants' group meeting on stable isotope reference samples for geochemical and hydrological investigations. Technical Report INIS-MF-10954, International Atomic Energy Agency (IAEA).
- Jaumann, R., Schmitz, N., Ho, T. M., Schröder, S. E., Otto, K. A., Stephan, K., Elgner, S., Krohn, K., Preusker, F., Scholten, F., Biele, J., Ulamec, S., Krause, C.,

Sugita, S., Matz, K. D., Roatsch, T., Parekh, R., Mottola, S., Grott, M., Michel, P., Trauthan, F., Koncz, A., Michaelis, H., Lange, C., Grundmann, J. T., Maibaum, M., Sasaki, K., Wolff, F., Reill, J., Moussi-Soffys, A., Lorda, L., Neumann, W., Vincent, J. B., Wagner, R., Bibring, J. P., Kameda, S., Yano, H., Watanabe, S., Yoshikawa, M., Tsuda, Y., Okada, T., Yoshimitsu, T., Mimasu, Y., Saiki, T., Yabuta, H., Rauer, H., Honda, R., Morota, T., Yokota, Y., and Kouyama, T. (2019) Images from the surface of asteroid Ryugu show rocks similar to carbonaceous chondrite meteorites. *Science* 365:817–820.

Jewitt, D. (2016) The Active Asteroids. Keck Observatory Archive LRIS U112L.

Junk, G. and Svec, H. J. (1958) The absolute abundance of the nitrogen isotopes in the atmosphere and compressed gas from various sources. *Geochim. Cosmochim. Acta* 14:234–243.

Kitazato, K., Milliken, R. E., Iwata, T., Abe, M., Ohtake, M., Matsuura, S., Arai, T., Nakauchi, Y., Nakamura, T., Matsuoka, M., Senshu, H., Hirata, N., Hiroi, T., Pilorget, C., Brunetto, R., Poulet, F., Riu, L., Bibring, J. P., Takir, D., Domingue, D. L., Vilas, F., Barucci, M. A., Perna, D., Palomba, E., Galiano, A., Tsumura, K., Osawa, T., Komatsu, M., Nakato, A., Arai, T., Takato, N., Matsunaga, T., Takagi, Y., Matsumoto, K., Kouyama, T., Yokota, Y., Tatsumi, E., Sakatani, N., Yamamoto, Y., Okada, T., Sugita, S., Honda, R., Morota, T., Kameda, S., Sawada, H., Honda, C., Yamada, M., Suzuki, H., Yoshioka, K., Hayakawa, M., Ogawa, K., Cho, Y., Shirai, K., Shimaki, Y., Hirata, N., Yamaguchi, A., Ogawa, N., Terui, F., Yamaguchi, T., Takei, Y., Saiki, T., Nakazawa, S., Tanaka, S., Yoshikawa, M.,

- Watanabe, S., and Tsuda, Y. (2019) The surface composition of asteroid 162173 Ryugu from Hayabusa2 near-infrared spectroscopy. *Science* 364:272–275.
- Kobayashi, K. (2019) *Prebiotic Synthesis of Bioorganic Compounds by Simulation Experiments*, page 43. Springer Nature (Singapore).
- Kojo, S. (2010) Origin of homochirality of amino acids in the biosphere. *Symmetry* 2:1022.
- Kolbe, E., Langanke, K., Martínez-Pinedo, G., and Vogel, P. (2003) Neutrino nucleus reactions and nuclear structure. *Journal of Physics G Nuclear Physics* 29:2569–2596.
- Koll, D., Korschinek, G., Faestermann, T., Gómez-Guzmán, J. M., Kipfstuhl, S., Merchel, S., and Welch, J. M. (2019) Interstellar ^{60}Fe in Antarctica. *Phys. Rev. Lett.* 123:072701.
- Krane, K. S. (1987) *Introductory Nuclear Physics*. Wiley-VCH (Weinheim).
- Lodders, K., Palme, H., and Gail, H. P. (2009) *Landolt-Brnstein - Group VI Astronomy and Astrophysics*, volume 4B, page 712. Springer Nature (Switzerland).
- Marhas, K. K., Goswami, J. N., and Davis, A. M. (2002) Short-Lived Nuclides in Hibonite Grains from Murchison: Evidence for Solar System Evolution. *Science* 298:2182–2185.
- Marty, B., Avice, G., Sano, Y., Altwegg, K., Balsiger, H., Hässig, M., Morbidelli, A., Mousis, O., and Rubin, M. (2016) Origins of volatile elements (H, C, N,

- noble gases) on Earth and Mars in light of recent results from the ROSETTA cometary mission. *Earth and Planetary Science Letters* 441:91–102.
- McDonough, W. F., Teng, F. Z., Tomascak, P. B., Ash, R. D., Grossman, J. N., and Rudnick, R. L. (2003) Lithium Isotopic Composition of Chondritic Meteorites. In Mackwell, S. and Stansbery, E., editors, *Lunar and Planetary Science Conference*, page 1931.
- Meierhenrich, U. (2008) *Amino Acids and the Asymmetry of Life*. Springer-Verlag (Berlin).
- Meyer, B. (2012) WEBNUCLEO.org. In *Nuclei in the Cosmos (NIC XII)*, page 96.
- Meyer, B. S., McLaughlin, G. C., and Fuller, G. M. (1998) Neutrino capture and r-process nucleosynthesis. *Phys. Rev. C* 58:3696–3710.
- Pizzarello, S. and Shock, E. (2010) The Organic Composition of Carbonaceous Meteorites: The Evolutionary Story Ahead of Biochemistry. *Cold Spring Harbor Perspectives in Biology* 2.
- Podlech, J. (2001) Origin of organic molecules and biomolecular homochirality. *Cellular and Molecular Life Sciences* 58:44–60.
- Rivera Islas, J., Micheau, J. C., and Buhse, T. (2004) *The Origin of Biomolecular Chirality*, pages 73–77. Springer Netherlands, Dordrecht.
- Rosswog, S. and Liebendörfer, M. (2003) High-resolution calculations of merging neutron stars - II. Neutrino emission. *Mon. Not. Roy. Astron. Soc.* 342:673–689.

- Sephton, M. A., Bland, P. A., Pillinger, C. T., and Gilmou, I. (2004) The preservation state of organic matter in meteorites from Antarctica. *Meteoritics and Planetary Science* 39:747–754.
- Sephton, M. A., James, R. H., Fehr, M. A., Bland, P. A., and Gounelle, M. (2013) Lithium isotopes as indicators of meteorite parent body alteration. *Meteoritics and Planetary Science* 48:872–878.
- Sojo, V. (2015) On the Biogenic Origins of Homochirality. *Origins of Life and Evolution of the Biosphere* 45:219–224.
- Strumia, A. and Vissani, F. (2003) Precise quasielastic neutrino/nucleon cross-section. *Physics Letters B* 564:42–54.
- Sugita, S., Honda, R., Morota, T., Kameda, S., Sawada, H., Tatsumi, E., Yamada, M., Honda, C., Yokota, Y., Kouyama, T., Sakatani, N., Ogawa, K., Suzuki, H., Okada, T., Namiki, N., Tanaka, S., Iijima, Y., Yoshioka, K., Hayakawa, M., Cho, Y., Matsuoka, M., Hirata, N., Hirata, N., Miyamoto, H., Domingue, D., Hirabayashi, M., Nakamura, T., Hiroi, T., Michikami, T., Michel, P., Ballouz, R. L., Barnouin, O. S., Ernst, C. M., Schröder, S. E., Kikuchi, H., Hemmi, R., Komatsu, G., Fukuhara, T., Taguchi, M., Arai, T., Senshu, H., Demura, H., Ogawa, Y., Shimaki, Y., Sekiguchi, T., Müller, T. G., Hagermann, A., Mizuno, T., Noda, H., Matsumoto, K., Yamada, R., Ishihara, Y., Ikeda, H., Araki, H., Yamamoto, K., Abe, S., Yoshida, F., Higuchi, A., Sasaki, S., Oshigami, S., Tsuruta, S., Asari, K., Tazawa, S., Shizugami, M., Kimura, J., Otsubo, T., Yabuta, H., Hasegawa, S., Ishiguro, M., Tachibana, S., Palmer, E., Gaskell, R., Le Corre, L., Jaumann, R., Otto, K., Schmitz, N., Abell, P. A., Barucci, M. A., Zolensky, M. E., Vi-

- Ias, F., Thuillet, F., Sugimoto, C., Takaki, N., Suzuki, Y., Kamiyoshihara, H., Okada, M., Nagata, K., Fujimoto, M., Yoshikawa, M., Yamamoto, Y., Shirai, K., Noguchi, R., Ogawa, N., Terui, F., Kikuchi, S., Yamaguchi, T., Oki, Y., Takao, Y., Takeuchi, H., Ono, G., Mimasu, Y., Yoshikawa, K., Takahashi, T., Takei, Y., Fujii, A., Hirose, C., Nakazawa, S., Hosoda, S., Mori, O., Shimada, T., Soldini, S., Iwata, T., Abe, M., Yano, H., Tsukizaki, R., Ozaki, M., Nishiyama, K., Saiki, T., Watanabe, S., and Tsuda, Y. (2019) The geomorphology, color, and thermal properties of Ryugu: Implications for parent-body processes. *Science* 364:252–252.
- Suzuki, T., Chiba, S., Yoshida, T., Kajino, T., and Otsuka, T. (2006) Neutrino-nucleus reactions based on new shell model Hamiltonians. *Phys. Rev. C* 74:034307.
- Suzuki, T., Chiba, S., Yoshida, T., Takahashi, K., and Umeda, H. (2018) Neutrino-nucleus reactions on ^{16}O based on new shell-model Hamiltonians. *Phys. Rev. C* 98:034613.
- Viedma, C., Ortiz, J. E., Torres, T. d., Izumi, T., and Blackmond, D. G. (2008) Evolution of solid phase homochirality for a proteinogenic amino acid. *Journal of the American Chemical Society* 130:15274–15275. PMID: 18954052.
- Watanabe, S., Hirabayashi, M., Hirata, N., Hirata, N., Noguchi, R., Shimaki, Y., Ikeda, H., Tatsumi, E., Yoshikawa, M., Kikuchi, S., Yabuta, H., Nakamura, T., Tachibana, S., Ishihara, Y., Morota, T., Kitazato, K., Sakatani, N., Matsumoto, K., Wada, K., Senshu, H., Honda, C., Michikami, T., Takeuchi, H., Kouyama, T., Honda, R., Kameda, S., Fuse, T., Miyamoto, H., Komatsu, G., Sugita, S., Okada,

T., Namiki, N., Arakawa, M., Ishiguro, M., Abe, M., Gaskell, R., Palmer, E., Barnouin, O. S., Michel, P., French, A. S., McMahon, J. W., Scheeres, D. J., Abell, P. A., Yamamoto, Y., Tanaka, S., Shirai, K., Matsuoka, M., Yamada, M., Yokota, Y., Suzuki, H., Yoshioka, K., Cho, Y., Tanaka, S., Nishikawa, N., Sugiyama, T., Kikuchi, H., Hemmi, R., Yamaguchi, T., Ogawa, N., Ono, G., Mimasu, Y., Yoshikawa, K., Takahashi, T., Takei, Y., Fujii, A., Hirose, C., Iwata, T., Hayakawa, M., Hosoda, S., Mori, O., Sawada, H., Shimada, T., Soldini, S., Yano, H., Tsukizaki, R., Ozaki, M., Iijima, Y., Ogawa, K., Fujimoto, M., Ho, T. M., Moussi, A., Jaumann, R., Bibring, J. P., Krause, C., Terui, F., Saiki, T., Nakazawa, S., and Tsuda, Y. (2019) Hayabusa2 arrives at the carbonaceous asteroid 162173 Ryugu—A spinning topshaped rubble pile. *Science* 364:268–272.

Woosley, S. E., Hartmann, D. H., Hoffman, R. D., and Haxton, W. C. (1990) The nu -Process. *Astroph. J.* 356:272.

Tables

Table 1: Neutrino temperatures (in MeV) and luminosities (10^{53} erg/s) for the three models used to compute the isotopic anomalies of the amino acids in this work. These parameters are taken from (Rosswog and Liebendörfer, 2003).

	Models		
	C	D	E
T_{ν_e}	4.2	4.1	5.0
$T_{\bar{\nu}_e}$	5.5	5.0	6.6
T_{ν_x}	8.9	6.6	9.1
L_{ν_e}	0.5	0.3	1.5
$L_{\bar{\nu}_e}$	1.5	0.9	2.25
L_{ν_x}	0.25	1	0.75

Table 2: Assumed initial mass fractions of isotopes for the carbonaceous chondrite (Lodders et al., 2009) and water inclusions in meteorites.

Isotope	CC	Water	Isotope	CC	Water
¹ H	3.74×10^{-2}	3.77×10^{-2}	¹² C	6.58×10^{-2}	5.96×10^{-2}
² H	1.45×10^{-6}	1.45×10^{-6}	¹³ C	8.00×10^{-4}	7.25×10^{-4}
³ He	2.18×10^{-12}	-	¹⁴ N	5.62×10^{-3}	5.10×10^{-3}
⁴ He	1.75×10^{-8}	-	¹⁵ N	2.21×10^{-5}	2.01×10^{-5}
⁶ Li	1.84×10^{-7}	-	¹⁶ O	0.888	0.894
⁷ Li	2.66×10^{-6}	-	¹⁷ O	3.50×10^{-4}	3.52×10^{-4}
⁹ Be	4.02×10^{-8}	-	¹⁸ O	2.00×10^{-3}	2.02×10^{-3}
¹⁰ B	2.72×10^{-7}	-	¹⁹ F	1.11×10^{-4}	-
¹¹ B	1.21×10^{-6}	-	²⁰ Ne	3.18×10^{-10}	-
			²¹ Ne	8.01×10^{-13}	-
			²² Ne	2.58×10^{-11}	-

Figure Legends

Figure 1: The weak interaction network used to evaluate isotopic abundance distributions in amino acid formation.

Figure 2: The abundance ratios compared to the measurements of (Elsila et al., 2012). Initial abundances are taken to be those of the Orgueil meteorite (Lodders et al., 2009) with isotopic fractions taken from the same reference. The symbols correspond to the results of Elsila, while the green, purple, and blue lines correspond to the results of the network calculation for models D, C, and E respectively. The source meteorite for each measurement is indicated by the symbol type, and the meteorite type is indicated by the symbol color. The direction of increasing integrated neutrino fluence is also shown as indicated. The black trefoil in each figure represents the arithmetic mean of the data.

Figure 3: The abundance ratios compared to the measurements of (Elsila et al., 2012). Initial abundances are taken to be those of the solar system at formation (Lodders et al., 2009) with isotopic fractions taken from the same reference. The symbols correspond to the results of Elsila, while the green, purple, and blue lines correspond to the results of the network calculation for models D, C, and E respectively. The source meteorite for each measurement is indicated by the symbol type, and the meteorite type is indicated by the symbol color. The direction of increasing integrated neutrino fluence is also shown as indicated. The black trefoil in each figure represents the arithmetic mean of the data.

Figure 4: The abundance ratios compared to the measurements of (Elsila et al., 2012). Initial abundances are taken to be current suggested solar system values (Lodders et al., 2009) with isotopic fractions taken from the same reference. The symbols correspond to the results of Elsila, while the green, purple, and blue lines correspond to the results of the network calculation for models D, C, and E respectively. The source meteorite for each measurement is indicated by the symbol type, and the meteorite type is indicated by the symbol color. The direction of increasing integrated neutrino fluence is also shown as indicated. The black trefoil in each figure represents the arithmetic mean of the data.

Figure 5: The abundance ratios compared to the measurements of (Elsila et al., 2012). Initial abundances are taken to be those of an inclusion with abundances given in the “water” column Table 2. The symbols correspond to the results of Elsila, while the green, purple, and blue lines correspond to the results of the network calculation for models D, C, and E respectively. The source meteorite for each measurement is indicated by the symbol type, and the meteorite type is indicated by the symbol color. The direction of increasing integrated neutrino fluence is also shown as indicated. The black trefoil in each figure represents the arithmetic mean of the data.

Figure 6: The isotopic ratios δD , $\delta^{13}C$, and $\delta^{15}N$ as a function of time (which corresponds to integrated neutrino flux) for cases in which neutron captures are disabled (dashed line) and in which subsequent neutron captures are disabled. In this figure, the neutrino flux corresponding to model E is assumed for an initial composition of the

solar system at the time of formation.

Figures

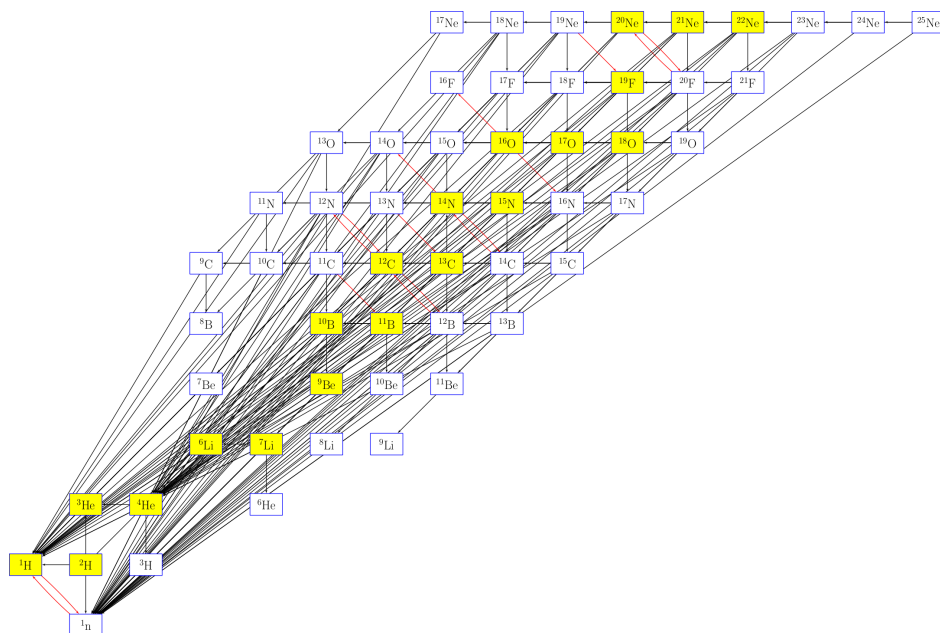


Figure 1: The weak interaction network used to evaluate isotopic abundance distributions in amino acid formation.

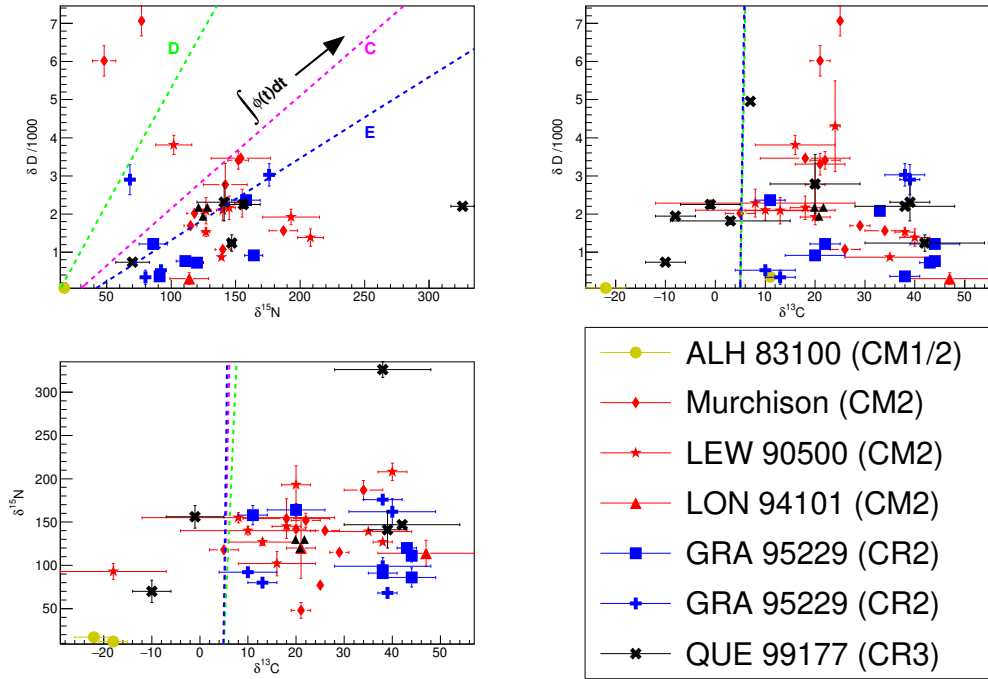


Figure 2: The abundance ratios compared to the measurements of (Elsila et al., 2012). Initial abundances are taken to be those of the Orgueil meteorite (Lodders et al., 2009) with isotopic fractions taken from the same reference. The symbols correspond to the results of Elsila, while the green, purple, and blue lines correspond to the results of the network calculation for models D, C, and E respectively. The source meteorite for each measurement is indicated by the symbol type, and the meteorite type is indicated by the symbol color. The direction of increasing integrated neutrino fluence is also shown as indicated. The black trefoil in each figure represents the arithmetic mean of the data.

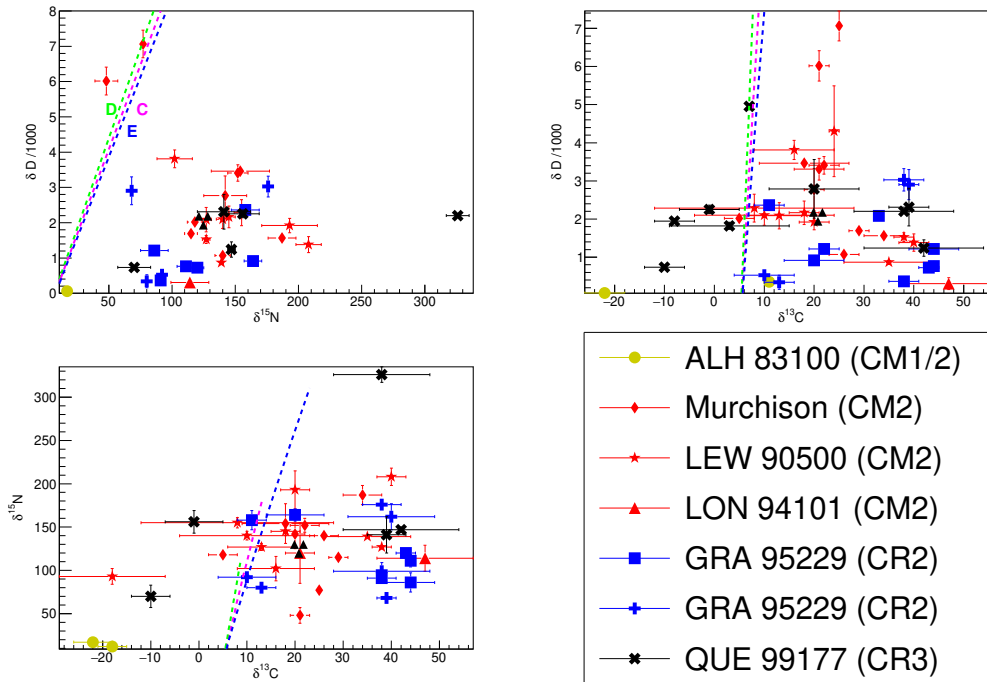


Figure 3: The abundance ratios compared to the measurements of (Elsila et al., 2012). Initial abundances are taken to be those of the solar system at formation (Lodders et al., 2009) with isotopic fractions taken from the same reference. The symbols correspond to the results of Elsila, while the green, purple, and blue lines correspond to the results of the network calculation for models D, C, and E respectively. The source meteorite for each measurement is indicated by the symbol type, and the meteorite type is indicated by the symbol color. The direction of increasing integrated neutrino fluence is also shown as indicated. The black trefoil in each figure represents the arithmetic mean of the data.

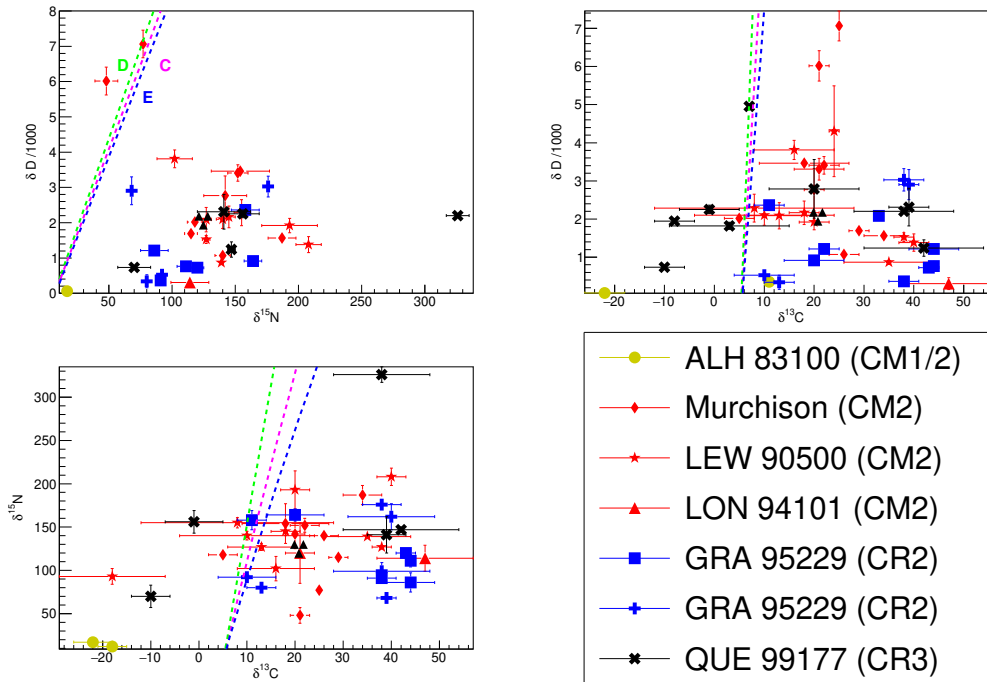


Figure 4: The abundance ratios compared to the measurements of (Elsila et al., 2012). Initial abundances are taken to be current suggested solar system values (Lodders et al., 2009) with isotopic fractions taken from the same reference. The symbols correspond to the results of Elsila, while the green, purple, and blue lines correspond to the results of the network calculation for models D, C, and E respectively. The source meteorite for each measurement is indicated by the symbol type, and the meteorite type is indicated by the symbol color. The direction of increasing integrated neutrino fluence is also shown as indicated. The black trefoil in each figure represents the arithmetic mean of the data.

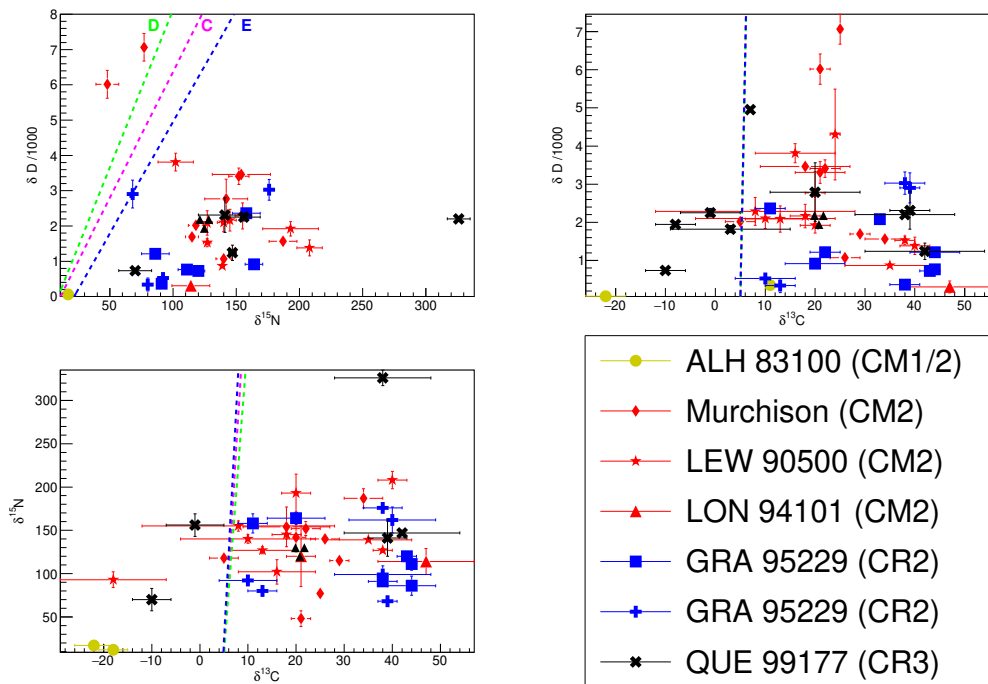


Figure 5: The abundance ratios compared to the measurements of (Elsila et al., 2012). Initial abundances are taken to be those of an inclusion with abundances given in the “water” column Table 2. The symbols correspond to the results of El-sila, while the green, purple, and blue lines correspond to the results of the network calculation for models D, C, and E respectively. The source meteorite for each measurement is indicated by the symbol type, and the meteorite type is indicated by the symbol color. The direction of increasing integrated neutrino fluence is also shown as indicated. The black trefoil in each figure represents the arithmetic mean of the data.

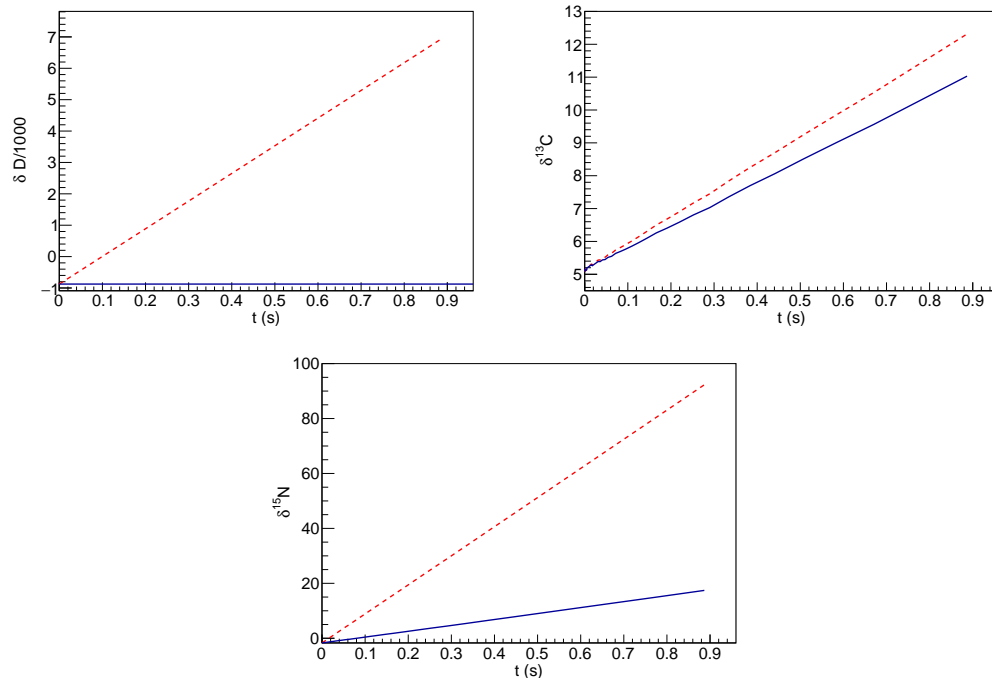


Figure 6: The isotopic ratios δD , $\delta^{13}C$, and $\delta^{15}N$ as a function of time (which corresponds to integrated neutrino flux) for cases in which neutron captures are present (dashed line) and in which subsequent neutron captures are disabled. In this figure, the neutrino flux corresponding to model E is assumed for an initial composition of the solar system at the time of formation.